

Collective Effects in Models for Interacting Molecular Motors and Motor-Microtubule Mixtures

Gautam I. Menon

*The Institute of Mathematical Sciences, C.I.T. Campus,
Taramani, Chennai 600 113, India*

Abstract

Three problems in the statistical mechanics of models for an assembly of molecular motors interacting with cytoskeletal filaments are reviewed. First, a description of the hydrodynamical behaviour of density-density correlations in fluctuating ratchet models for interacting molecular motors is outlined. Numerical evidence indicates that the scaling properties of dynamical behavior in such models belong to the KPZ universality class. Second, the generalization of such models to include boundary injection and removal of motors is provided. In common with known results for the asymmetric exclusion processes, simulations indicate that such models exhibit sharp boundary driven phase transitions in the thermodynamic limit. In the third part of this paper, recent progress towards a continuum description of pattern formation in mixtures of motors and microtubules is described, and a non-equilibrium “phase-diagram” for such systems discussed.

1 Introduction

Living systems exhibit a remarkable variety of non-equilibrium steady states. Problems associated with the modelling of such states include the description of the non-equilibrium behaviour of membranes driven by active pumps[1], hydrodynamic approaches to the motion of self-propelled objects[2,3], the theory of pattern formation in a variety of biological contexts[4] and models for intracellular transport processes associated with the motion of molecular motors[5]. This last problem has attracted the attention of statistical physicists in recent years, since the simplest models for such systems have several advantages: they are exactly solvable even in the presence of interactions, easy to generalize,

Email address: menon@imsc.res.in (Gautam I. Menon).

relatively straightforward to simulate and closely related to models studied extensively in the context of traffic flow[5].

It is useful to develop intuition with simple models, requiring only that it should be possible to add the requisite biological detail incrementally. This would then allow progressively more accurate descriptions to be constructed within a sequence of increasingly refined models. This paper reviews some calculations which explore the middle ground between extremely simplified statistical mechanics models for the motion of interacting molecular motor proteins – the asymmetric exclusion process and generalizations – and marginally more realistic models for the motion of individual motor proteins generalized to accommodate motor-motor interactions[6]. It also reviews some recent work on the hydrodynamic description of pattern formation in mixtures of molecular motors and microtubules[7].

Molecular motors are a class of biological machines which function within cells[8]. Such motors, proteins such as kinesins, myosins and dyneins, move unidirectionally on one-dimensional “tracks” while hydrolysing adenosine triphosphate (ATP). These tracks are components of the cytoskeleton in eukaryotic cells, an extended dynamic network formed through the polymerization and crosslinking of tubulin and actin monomers to form microtubules and actin filaments[9]. The cytoskeleton helps the cell anchor to substrates, to move and to divide, and lends it mechanical and structural rigidity. In addition, this network defines paths for molecular motors to transport cargo to different parts of the cell[9].

The asymmetric nature of motor motion along the cytoskeleton derives from the asymmetry of the constituent monomeric units of the track. Microtubules (equivalently, actin filaments) can be idealised as periodic, one-dimensional, rigid structures, this periodicity following from their polymeric nature. The violation of detailed balance necessary in order for the motor to exhibit directed motion comes from the transduction of the chemical energy obtained from ATP hydrolysis into mechanical work[10]. The stochastic uptake of ATP is one source of random noise in the problem; the other is the thermal noise which dominates all biological systems at cellular scales. Molecular motors thus act as *Brownian rectifiers* in exhibiting a non-zero drift velocity in the absence of a net time-averaged force. The problem of modelling molecular motors can therefore be placed in the more general context of “Brownian motor” or “thermal ratchet” models for the extraction of useful work from thermal fluctuations[10,11].

We consider the “fluctuating potential” or “flashing ratchet” model for Brownian motors[10]. In this model, a single motor, idealized as a point object moving in one dimension, is driven by stochastic forces uncorrelated in space and time and drawn from a Gaussian distribution with zero mean. The motor

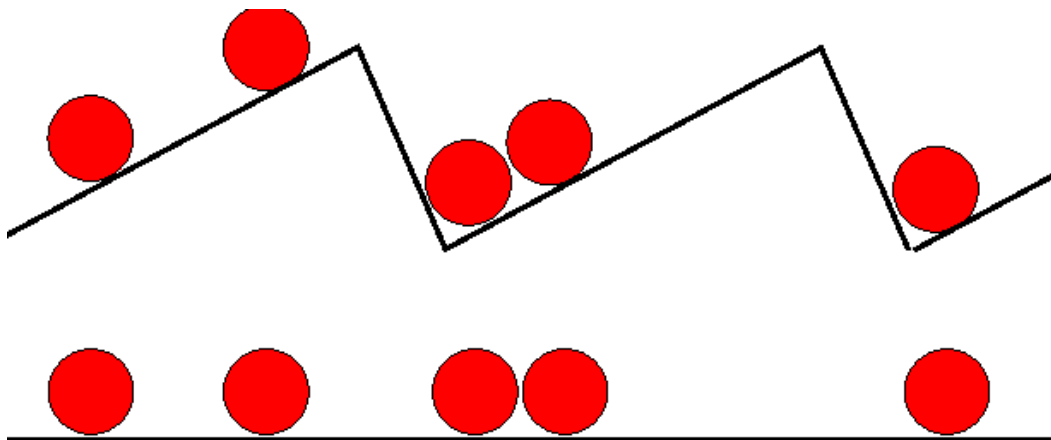


Fig. 1. The continuum potential corresponding to the two states (non-trivial and flat) of the potential, showing the locations of several motors interacting through a hard-core repulsive potential.

also experiences a force derived from the gradient of a time-dependent potential. The time dependence of this potential is generated by switching randomly between two states, one in which the potential is an asymmetric sawtooth – say with the longer leg of the potential to the left – and the other in which it is flat.

In the “off” or “flat” state of the potential, particles diffuse isotropically. When the potential is switched to the “on” state, a particle is more likely to be found in a region of space where it experiences a net force to the left than to the right, given that the potential lacks right-left symmetry. Repeated cycling between “off” and “on” states generates net motion. The generation of directed motion occurs through a subtle mechanism: in any one of the potential states, given sufficient time to equilibrate, no net current can flow provided the microscopic jump rates obey detailed balance. The breaking of detailed balance overall arises from the non-equilibrium, time-dependent *switching* between potential states and not from the choice of hopping rates in any one of these states [10].

In modelling biological motors, the asymmetric potential encodes the energy associated with an internal state of the motor as a function of its position along the track[10]. This state represents a particular conformation of the motor protein. ATP consumption induces transitions between states. A motor molecule thus has two degrees of freedom, a spatial coordinate and an internal (state) coordinate. A faithful representation of the internal states of the motor and track thus involves specifying a large number of continuous periodic potentials representing the energy of a molecular motor at location x as a function of its state s .

The simplified model described here retains only two states of the motor-track complex. Such “minimal” models may be expected to capture some of the relevant complexity of the real biological system, at least in the limited

contexts in which we will study them. It is straightforward to generalize the models described here. In particular, one could allow motors both to detach from the filament and diffuse within the ambient solvent as well as to reattach with prescribed rates. One could also allow for motors of finite extent, by extending the exclusion constraint to sites which neighbour the one occupied by the motor.

The effects of cooperativity between motors has been a source of rich physics in recent years [10,12,13,14,15]. Such effects, in biological models for the action of the myosin motors involved in muscle contraction, have been incorporated by coupling motors through intervening elastic elements. Thus, in addition to forces derived from the external potential and Gaussian noise, a motor feels a force due to its elastic interactions with its neighbours. A mean-field analysis of the effects of such elastic couplings yields a variety of novel phenomena, such as Hopf bifurcations and spontaneous oscillations of the current[10]. However, another class of interaction effects which operate between elastically decoupled motors can be envisaged: the steric hindrance (or, in general, any short-range interaction) experienced by motors translocating on a filament when they approach each other[16,6,17].

How can the fluctuating potential model be generalized to incorporate the effects of interactions between many motors moving on a cytoskeletal filament? The simplest such interaction is a hard-core interaction between two motors, as illustrated schematically in Fig 1. On the lattice, this constraint is simply implemented by allowing only one particle to occupy a given lattice site at a time. We define simple lattice models incorporating such interactions and study these models with boundary conditions (periodic) which conserve the total number of motors in Section II. We also discuss a simple mean-field theory and its prediction for currents and density profiles within a single period of the potential. A second set of results, presented in Section III, relate to the existence of phase transitions in such systems induced by the effects of adding (subtracting) motors at the boundaries of the (open) one-dimensional chain at prescribed rates[18]. Our numerically calculated phase diagram closely resembles the phase diagram of the partially asymmetric exclusion process with boundary driving[19,20].

The fact that these two systems should be related at the level of hydrodynamic correlations was conjectured in Ref.[6] and used to predict that density-density correlations in the steady state of the interacting motor system should obey scaling with exponents belonging to the KPZ universality class. The fact that these systems show the same type of phase transitions as a function of boundary conditions is further evidence of the close relationship between these models, despite the far greater complexity (multiplicative time and space-dependent noise at the level of the microscopic hopping rates) in the Brownian motor model.

A third set of results reviewed in this paper (Section IV) relate to the modelling of the patterns which form when motor complexes are mixed with microtubules and supplied with ATP, in a quasi-two-dimensional geometry[7]. These patterns include structures such as asters, vortices and aster-vortex mixtures as well as disordered states. Understanding the generic features of these states, the sequence of transformations between them as a function of the motor density and the interactions which contribute to the formation of such self-organized structures, is believed to be a crucial part of understanding the physics behind the formation of a cellular-scale pattern universal to all eukaryotic cells, the mitotic spindle [21,22,23,24,25,26,27]. The concluding section, Section V, discusses some general features of the results, suggesting that the general attribute of “physical robustness”, a robustness of the non-equilibrium steady states obtained in such models towards a wide class of physically relevant perturbations, may be biologically relevant.

2 KPZ Scaling in Interacting Ratchet Models

In the simplest continuum versions of the fluctuating potential models, individual motor particles see a time-dependent potential $V(x, t) = \eta(t)U(x)$, in addition to random Brownian forces with zero mean value. Here $U(x)$ is periodic with period ℓ *i.e.* $U(x + \ell) = U(x)$ and an asymmetric function of x *i.e.* $U(x) \neq U(-x)$. The time dependence of $V(x, t)$ is governed by a (stochastic or deterministic) switching function $\eta(t)$ which takes the values 0 and 1. We assume $U(x)$ to be of the sawtooth form

$$\begin{aligned} U(x) &= ax & (0 \leq x \leq \omega\ell), \\ &= b(\ell - x) & (\omega\ell \leq x \leq \ell) \end{aligned} \tag{1}$$

with $a, b > 0$, $a\omega\ell = b\ell(1 - \omega)$ and $\omega < 1$. The switching of the potential occurs independently of the state of the motors, thus breaking detailed balance. Together with the lack of reflection symmetry in $U(x)$, this switching generates a net particle current.

A useful simplification is the discretization of the periodic potential in space to convert the continuum problem into a lattice one. (This is not a unreasonable simplification, since the biological motor appears to undergo a sequence of *discrete* conformational changes, each of which is coupled to a partial translocation across the period.) Each period of the potential is divided into W lattice sites, all of which are assigned to the segment of the potential with positive slope. The length of the system, L , is measured in periods of the sawtooth. The maximum height of the sawtooth potential is V and we define $r = \exp(-\frac{V}{k_B T(W-1)})$. Finally, the parameters P_{01} and P_{10} represent the

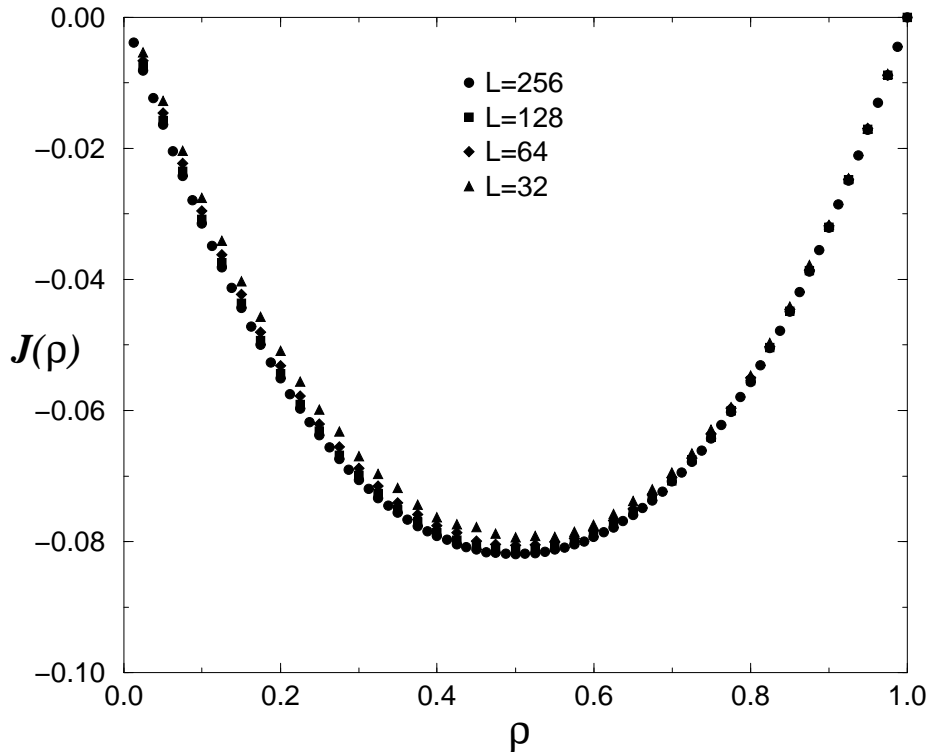


Fig. 2. Dependence of the steady-state current on the density ρ of particles for $32 \leq L \leq 256$.

probabilities that the potential changes from $\eta = 0$ to $\eta = 1$ and vice versa.

The transition rates between the configurations of motors are chosen to satisfy detailed balance with Metropolis rates, $P(\{\sigma'\} \rightarrow \{\bar{\sigma}\}) = \min(1, \exp[H(\{\sigma'\}) - H(\{\bar{\sigma}\})])$. Here $\{\sigma\}$ indexes allowed configurations of the motors on the lattice and $H(\{\sigma\})$ is the energy of the configuration. In terms of these parameters the hopping probabilities for motor particles on the sawtooth are

$$\begin{aligned}
 P(i \rightarrow i+1) &= \begin{cases} \frac{r}{1+r} & \text{if } 0 \leq i < W-1 \\ \frac{1}{1+r^{W-1}} & \text{if } i = W-1, \end{cases} \\
 P(i+1 \rightarrow i) &= \begin{cases} \frac{1}{1+r} & \text{if } 0 \leq i < W-1 \\ \frac{r^{W-1}}{1+r^{W-1}} & \text{if } i = W-1, \end{cases} \quad (2)
 \end{aligned}$$

where we have indexed the lattice sites from 0 at the potential minimum. The hopping probabilities for left(right) jumps on the flat potential equal $1/2$ at every site.

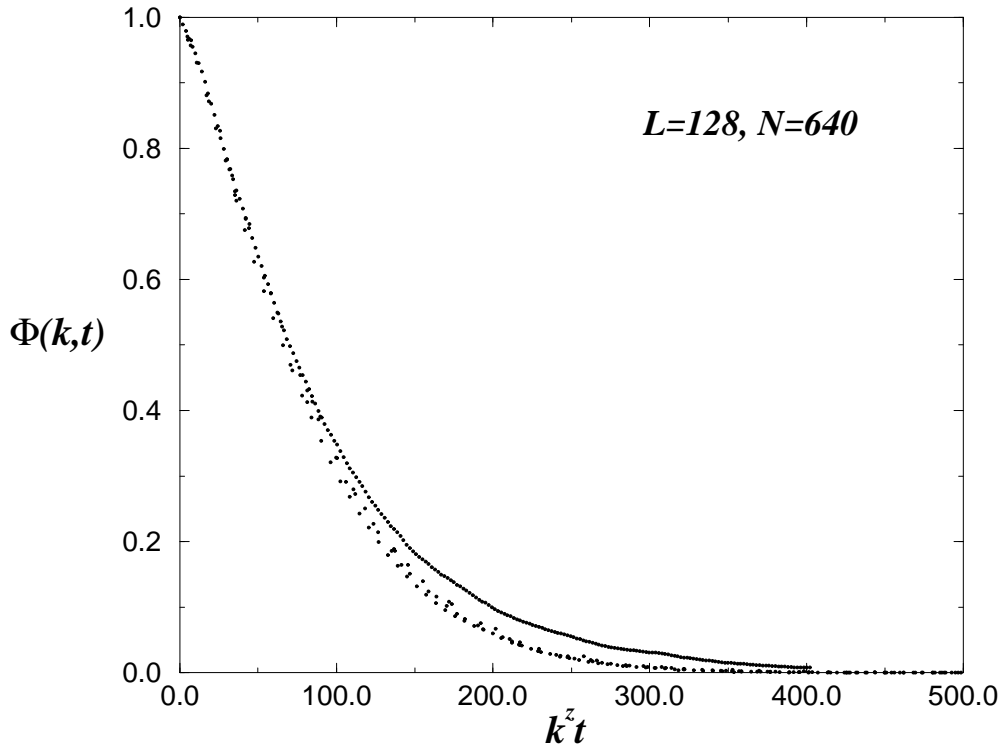


Fig. 3. The relaxation function $\Phi(k, t)$ for $L = 128$ and $\rho = 0.5$ plotted as a function of the scaled variable $k^z t$ for $z = 1.60$ for the five smallest values of $k = 2\pi j/L$, with $j = 1, 2, 3 \dots$. The lowest k -value splits off whereas data for all higher k fall on the same branch.

To generalize models for single Brownian motors to a finite number N_p of interacting motors on a one-dimensional lattice, we assume that these motors hop to unoccupied nearest neighbour sites with rates determined by the discretized potential in Eq. (2), exactly as they would in the non-interacting case. The only interaction between these motors is thus a hard-core repulsion which prevents them from occupying the same lattice site. Our discretization and the hard-core constraint ensures an upper bound on the number of motors which can occupy the lattice.

We consider periodic boundary conditions in the calculations described in this section. Our motors thus move on a ring. An elementary step consists of either an attempt of a particle to hop to a neighbouring site or an attempt to switch the potential state globally. The results of Ref. [6] were obtained by a procedure which involved changing the potential state globally. Flipping this state locally does not alter the conclusions qualitatively and the quantitative changes are small.

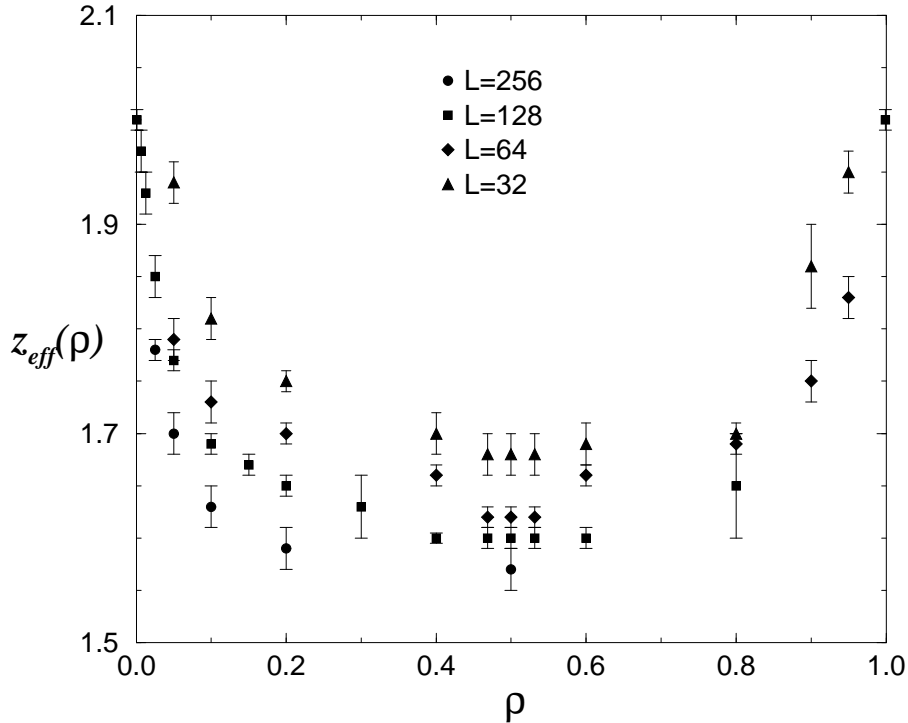


Fig. 4. The effective exponent $z_{eff}(N, \rho)$ plotted as function of ρ for systems of size $32 \leq L \leq 256$. Note the systematic decrease of z_{eff} as L is increased at constant density.

Numerical results for the model defined above (Model I of Ref. [6]) are obtained in the following way: We use $W = 10$ lattice sites per period of the asymmetric sawtooth in all our simulations, varying the system size $L = 24, 48, 64, 128, 256$ and 512. We took $r = 0.05$, $P_{01} = 0.03$ and $P_{10} = 0.04$, where P_{01} and P_{10} are the probabilities that the potential state goes from flat to non-flat and vice versa. Typically, the system equilibrates over 5×10^4 MCS before data for currents and correlation functions are recorded. These quantities are averaged over $5 \times 10^3 - 10^4$ configurations.

Fig. 2 illustrates the fundamental relation (the functional dependence of the current on the density) of the model. We examine principally the scaling properties of the intermediate scattering function $S_\rho(k, t)$ defined by

$$S_\rho(k, t) = \frac{1}{N} \langle \delta\rho(k, 0) \delta\rho(-k, t) \rangle, \quad (3)$$

where N is the number of particles, k is $2n\pi/L$, $n = 0, \pm 1, \pm 2, \dots, L/2$, and L is the system size. Here $\delta\rho(k, t)$ is the Fourier component with wave vector

k of the deviation from the mean local density, $\delta\rho(x, t) = \rho(x, t) - \langle \rho(x) \rangle$, with the brackets $\langle \cdot \rangle$ denoting a time average.

Transforming the density field $\rho(x, t)$ to a “height” field $h(x, t)$ via $\rho(x, t) = \partial_x h(x, t)$, and imposing helical boundary conditions on $h(x, t)$ to satisfy the constraint $\int_0^L \rho(x, t) dx = h(L) - h(0) = N$, $S_\rho(k, t)$ can be related to the structure factor $S(k, t) = \langle \delta h(k, 0) \delta h(-k, t) \rangle$ where $\delta h(k, t)$ is the Fourier transform of $h(x, t) - \langle h(x) \rangle$. For small k and large t , *i.e.* in the hydrodynamic limit, if $S(k, t)$ exhibits dynamical scaling, we can write $S(k, t) \sim k^{-2+\eta} F(k^z t)$, where η and z are scaling exponents and F is a scaling function.

In Ref.[6], it was conjectured that the dynamical scaling properties of the “height” field should be described by the Kardar-Parisi-Zhang [28] equation, a non-linear Langevin equation of the form,

$$\frac{\partial h}{\partial t} = \nu \nabla^2 h + \frac{\lambda}{2} (\nabla h)^2 + \zeta(\mathbf{x}, t), \quad (4)$$

which is known to describe the long-time, long-wavelength behavior of a number of nonequilibrium systems [29]. This equation is written in a form appropriate for surface models where $h(\mathbf{x}, t)$ is the height, relative to a d -dimensional substrate, of a growing interface and $\zeta(\mathbf{x}, t)$ represents white noise. For the KPZ equation, owing to the existence of a fluctuation-dissipation theorem, the exponents can be obtained exactly for $d = 1$ and take on the values $z = 3/2$ and $\eta = 0$. The connection is made in the following way: Coarse-grain microscopic configurations of such models in space and time. At spatial scales larger than the repeat distance ℓ of the periodic potential and for time scales much larger than the typical time-scale τ over which the potential changes, the system will appear to have a constant density on average, as well as a constant current. Superimposed on this constant density are spontaneous fluctuations which obey a local conservation law. The effects of interparticle interactions at the largest length scales can be summarized in the following observation: These density fluctuations are convected with a speed, the “kinematic wave speed”, which depends on their magnitude.

Consider now the statistical mechanics of an unrelated model, that of the stochastic dynamics of a finite density ρ of hard-core particles on a line, which hop individually with rate $(1 + \epsilon)/2$ to the right and $(1 - \epsilon)/2$ to the left, provided the excluded volume constraint is satisfied is known as the “asymmetric exclusion process” (ASEP) for $\epsilon \neq 0$. The ASEP has a net particle current $J = \epsilon\rho(1 - \rho)$. The symmetry breaking which results in a constant current in the ASEP is an explicit consequence of the asymmetry in the hopping rates. This symmetry breaking is to be contrasted to the more subtle symmetry breaking in the case of the ratchet models.

Density-density correlations for the ASEP are known to be governed by KPZ exponents[30,31,32]. Since both models share the feature expected to be most relevant to a hydrodynamic description – the existence of a non-trivial density-dependent current – it is reasonable to conjecture that they should belong to the same universality class, irrespective of the fact that the detailed origin of the symmetry breaking is different in each case.

In our simulations we measured the relaxation function [30]

$$\Phi(k, t) \equiv \frac{\langle \hat{\rho}(-k, 0) \hat{\rho}(k, t) \rangle - \langle \hat{\rho}(-k, 0) \rangle \langle \hat{\rho}(k, t) \rangle}{\langle \hat{\rho}(-k, 0) \hat{\rho}(k, 0) \rangle - \langle \hat{\rho}(-k, 0) \rangle \langle \hat{\rho}(k, 0) \rangle} = \frac{S_\rho(k, t)}{S_\rho(k, 0)}, \quad (5)$$

which is just the Fourier transform of $\sum_i (\rho_i(t) - \rho_i(0))(\rho_{j+i}(t) - \rho_{j+i}(0))$, normalised by its value at $t = 0$, an arbitrarily chosen time in the steady state. The data for $\Phi(k, t)$ for a given density and system size were plotted as a function of the scaled variable $k^z t$ for various z and the value of z that provided the best collapse of the data by visual inspection was taken to be z_{eff} . Examples of this data collapse are shown in Fig 3 at half filling for $L = 128$ for $z_{eff} = 1.60$. The relaxation function generically has two distinct branches: For the smallest value of k , $k = 2\pi/L$, the relaxation function decays more slowly than for larger values of k . For $j > 1$ the data collapse to quite high accuracy onto a single curve. This separation of the relaxation function into two branches (with $j = 1$ the special case) is also a feature of the single step model[33].

We have carried out this analysis systematically for $L = 32$ to $L = 256$ as function of ρ . The effective exponents $z_{eff}(N, \rho)$ are plotted as functions of ρ in Fig. 4. There is a systematic decrease of the effective exponent z_{eff} as function of increasing L for all $\rho \neq 0$, with the smallest values occurring at $\rho = 0.5$, as expected on theoretical grounds. The smallest value of the critical exponent, z , from this data was found to be $1.58 \pm .01$ for $L = 256$. Extrapolating to the thermodynamic limit, $z(\rho)$ approaches the function:

$$z = \begin{cases} \frac{3}{2} & \text{for } 0 < \rho < 1 \\ 2 & \text{for } \rho = 0, 1. \end{cases},$$

consistent with the predictions of the KPZ equation.

2.1 Mean-Field Approximation

Assuming periodic boundary conditions, all periods of the potential are equivalent in steady state. By translational invariance, it is then sufficient to solve

for the steady state density fields and steady-state currents within a single period. If a site is to be updated, which is the case with probability $1/2$ in each elementary time step, the density $\rho_i(t)$ at site i at time t changes through hops on and off that site from neighbouring sites. These hops can only occur if the hard-core constraint is satisfied. Allowed hops occur with the (microscopic) probabilities $p_i^L(t)$ and $p_i^R(t)$ for hops to the left ($p_i^L(t)$) or right ($p_i^R(t)$) at site i at time t . Given our algorithm, in which an attempt is made to update either a particle or a potential state at each time step and never both, the assignment of particle hopping rates at time t is unambiguous. However, how these rates are to be interpreted in the time-continuum limit is not straightforward and will be dealt with explicitly in what follows.

The update processes for a site i at time t can be written purely in terms of the local density fields in the neighbourhood of that site. The density field $\rho_i(t+1)$ at time $t+1$ is given by :

$$\rho_i(t+1) = \begin{cases} \rho_i(t) & \text{Probability } (1 - 3/N) \\ \rho_i(t) & \text{Probability } (1 - p_{i-1}^R)/N \\ \rho_i(t) + (1 - \rho_i(t))\rho_{i-1}(t) & \text{Probability } p_{i-1}^R/N \\ \rho_i(t) & \text{Probability } (1 - p_i^R - p_i^L)/N \\ \rho_i(t)\rho_{i-1}(t) & \text{Probability } p_i^L/N \\ \rho_i(t)\rho_{i+1}(t) & \text{Probability } p_i^R/N \\ \rho_i(t) & \text{Probability } (1 - p_{i+1}^L)/N \\ \rho_i(t) + (1 - \rho_i(t))\rho_{i+1}(t) & \text{Probability } p_{i+1}^L/N \end{cases} \quad (6)$$

The first term in Eq. (6) represents the probability that a site other than i is picked at time step t , whereas subsequent terms represent probabilities that the density variable at site i is updated as a consequence of site $i-1$, i or $i+1$ being picked. An overall factor of $1/2$ in these transition probabilities (arising from the fact that the choice to update a site or potential is made with probability $1/2$ at every time step), has been absorbed into a rescaling of time.

The hopping rates p_{i-1}^R , p_i^R , p_i^L , p_{i+1}^L are all explicitly functions of time and are determined by the instantaneous state of the potential. This state is determined by a corresponding equation for the dynamics of the potential field or equivalently of the stochastic variable $\eta(t)$ which appears in the definition of $V(x, t)$. We must specify two averages in the steady state. One is the average over thermal noise given a *particular* stochastic history of potential flips. The other is the average over all stochastic histories. We are interested in those

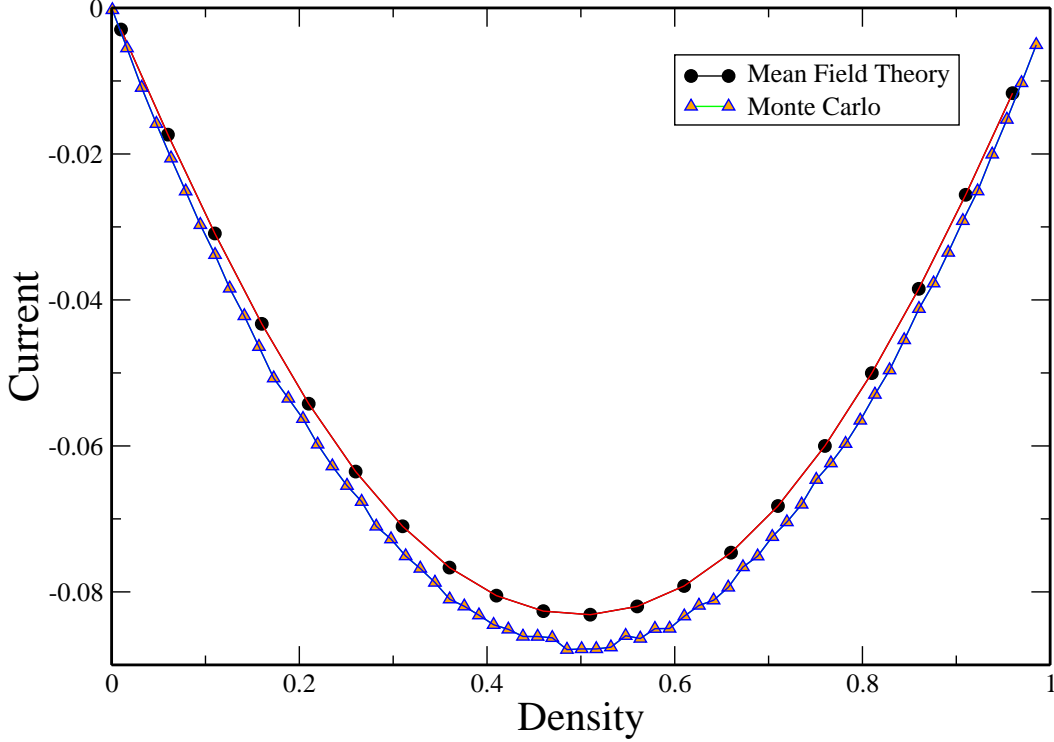


Fig. 5. The current-density relation as obtained through Monte Carlo simulations and the mean field theory described in the text, assuming $r = 0.05$, $P_{01} = 0.03$ and $P_{10} = 0.04$.

attributes of the system which characterize its steady state. The dynamics of potential and particle are partially decoupled. The potential state influences the particle hopping rate but the potential flips independently of the particle state. The mean-field approximation made is the following: Whenever a product such as $\rho_i(t)\rho_{i+1}(t)$ is to be averaged over either thermal noise or potential flip histories (with the appropriate averaging operation denoted by $\langle \cdot \rangle$), we replace $\langle \rho_i(t)\rho_{i+1}(t) \rangle$ by $\langle \rho_i(t) \rangle \langle \rho_{i+1}(t) \rangle$. This approximation truncates the hierarchy of coupled correlation functions by representing correlation functions of all higher-order products of density fields in terms of single-site averages. Our mean-field theory is formulated for the following limit: If the potential fluctuates over a microscopic time-scale which is much faster than characteristic diffusion time scales over a single period, it is legitimate to *average* the rates. The discrete equation Eq. (6), can then be converted into a first-order non-linear system of differential equations in time. These equations are

$$\frac{d\rho_i(t)}{dt} = \tau_i^1 \rho_i(t) + \tau_i^2 \rho_{i-1}(t) + \tau_i^3 \rho_{i+1}(t) + \tau_i^4 \rho_{i-1}(t)\rho_i(t) + \tau_i^5 \rho_i(t)\rho_{i+1}(t) \quad (7)$$

where i runs over the sites in a single period. Given P_{01} and P_{10} , the definitions of $\tau_i^1 \dots \tau_i^5$ are the following: $\tau_i^1 = -\bar{p}_i^L - \bar{p}_i^R$, $\tau_i^2 = \bar{p}_{i-1}^R$, $\tau_i^3 = \bar{p}_{i+1}^L$, $\tau_i^4 = \bar{p}_i^L + \bar{p}_{i-1}^R$ and $\tau_i^5 = \bar{p}_i^R + \bar{p}_{i+1}^L$. The bars denote an average over the rates. The set of

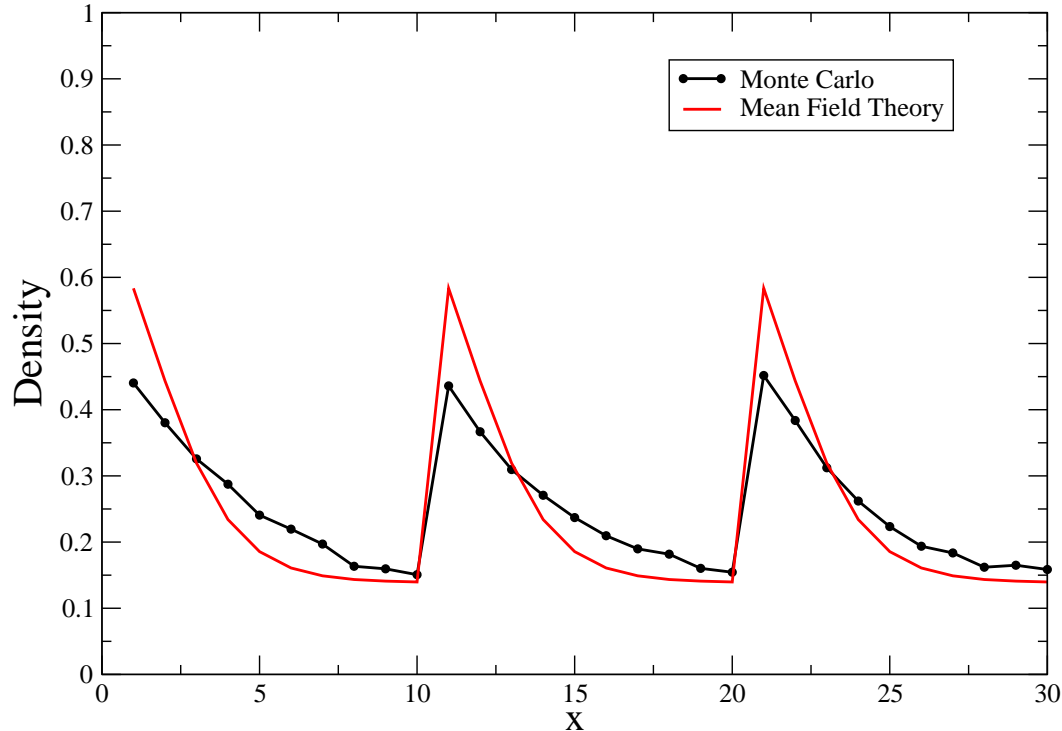


Fig. 6. The comparison between local densities in each period as obtained by averaging the Monte Carlo data and predictions of the mean field theory described in the text, assuming $r = 0.05$ $P_{01} = 0.03$ and $P_{10} = 0.04$. The mean density is 0.25.

equations Eq.(7) represent the mean-field treatment of the case in which the average over stochastic histories of potential flips has been performed before the average over thermal histories. The steady state in mean-field theory is obtained by setting the time derivatives $d\rho_i(t)/dt$ to zero. The resulting equations are to be solved for the W sites within a period, Given a mean field solution for the densities, the time-averaged current in the mean-field approximation can be obtained. Fig 5 illustrates the comparison of the fundamental diagram of the system as obtained through the mean field theory with the Monte Carlo data. The density profiles for densities 0.25 and 0.75 are shown in Figs. 6 and 7 together with the results of a direct numerical simulation. It can be seen that the mean-field theory in the averaged-rate limit used above predicts the currents and the density profiles to reasonable accuracy. At the level of the currents, the agreement between the mean-field theory and the simulation results is certainly passable. The density profiles appear qualitatively accurate but are incorrectly rendered in quantitative terms.

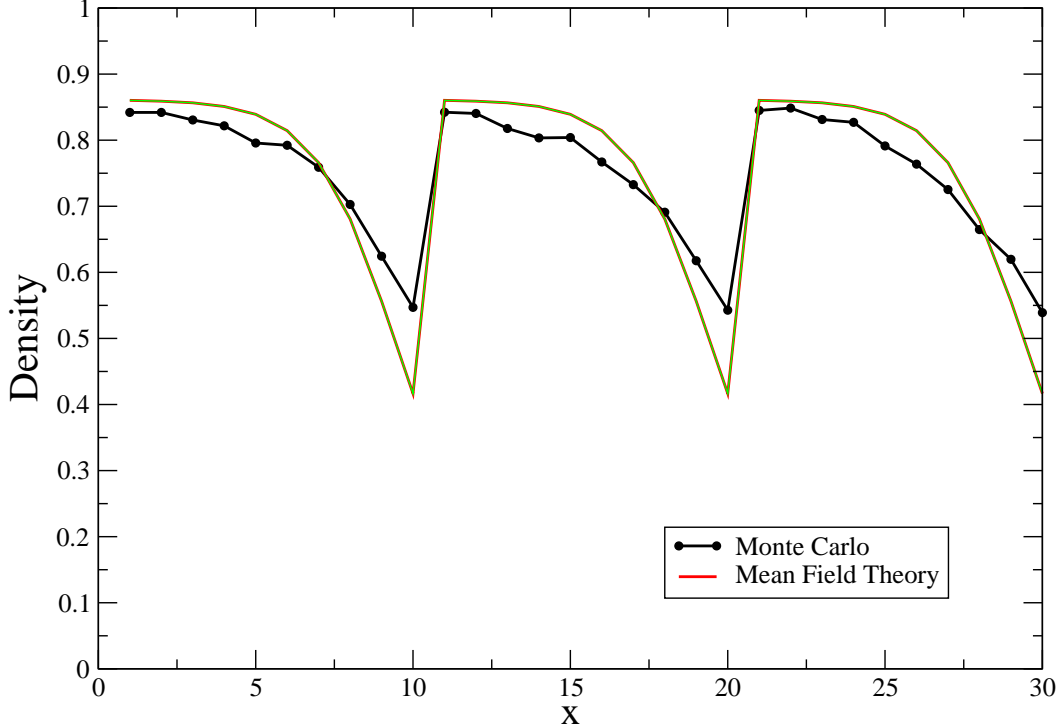


Fig. 7. The comparison between local densities in each period as obtained by averaging the Monte Carlo data and predictions of the mean field theory described in the text, assuming $r = 0.05$ $P_{01} = 0.03$ and $P_{10} = 0.04$. The mean density is 0.75.

3 Boundary-Driven Phase Transitions

The periodic boundary condition assumed in previous sections is clearly incorrect in the biological context, where motors are loaded and unloaded along the cytoskeleton at rates dictated by the local chemistry. As the two ends of a cytoskeletal filament loaded with motors carrying cargo are potentially well separated in space, their chemical environments need not be identical. It is thus possible that motor *loading* and *unloading* rates could be different at either end of the filament. The generalization of ratchet models for the motion of interacting motors, extended to allow for open boundary conditions, could potentially allow for the boundary injection and removal of motors. This injection and removal will compete, in general, with the bulk equilibration via Langmuir kinetics[34,35,36] of the motor density along the filament, but we will ignore the possibility that motors are lost or gained along the filament, accounting only for their entry and exit at the boundaries. For recent work which incorporates both bulk non-conservation and the effects of geometry, see Refs. [37,38,39,40,41].

For simulations with open boundary conditions, we attach two boundary sites to the open chain with N sites; the total number of sites is then $N + 2$. These boundary sites are filled with probability α (at the right boundary) or β (at the

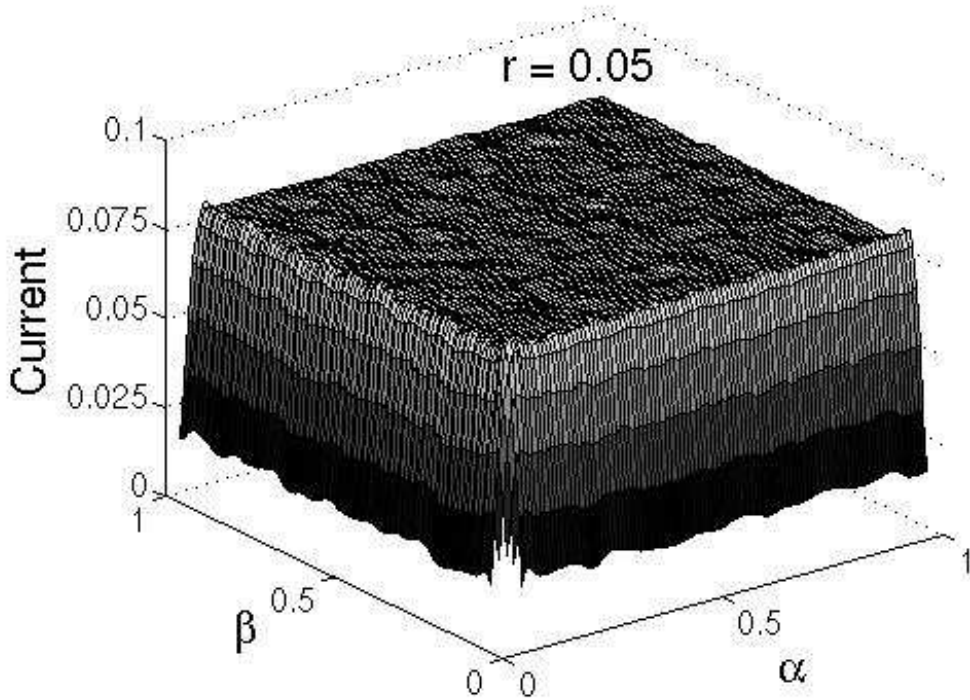


Fig. 8. Current versus the boundary and injection rates α and β , obtained through Monte Carlo simulations for parameter values $N = Lw = 128 * 10$ sites, $r = 0.05$, $P_{10} = 0.04$ and $P_{01} = 0.05$.

left boundary). Hopping rules at these special sites are chosen to be consistent with the direction of the net current in the absence of boundary driving and motors at these singled-out sites always hop unidirectionally. Results for this model are shown in Fig 8 which exhibits the current in the system J as a function of the input and output rates, α and β . Note the striking feature of the plot – the remarkable independence of J on α and β for a wide range of these parameters. For this range of input and output rates, the current is not only *independent* of the rates at which motors are added or subtracted at both ends but the current being passed through the system is pegged at its *maximum* value. Fig. 9 shows the steady state densities at varying input and output rates.

Note the existence of three distinct phases: (I) a phase in which the current and density can be varied by changing only β and is independent of α , (II) a phase in which the current and density can be varied by changing only α and is independent of β , (III) a “constant current” phase in which the current attains its maximum possible value and is independent of both α and β . The boundary driven ASEP has a phase diagram which is qualitatively very closely similar, with a low density phase, a high density phase and a intermediate constant current phase[20]. It should, in principle be possible to investigate the same

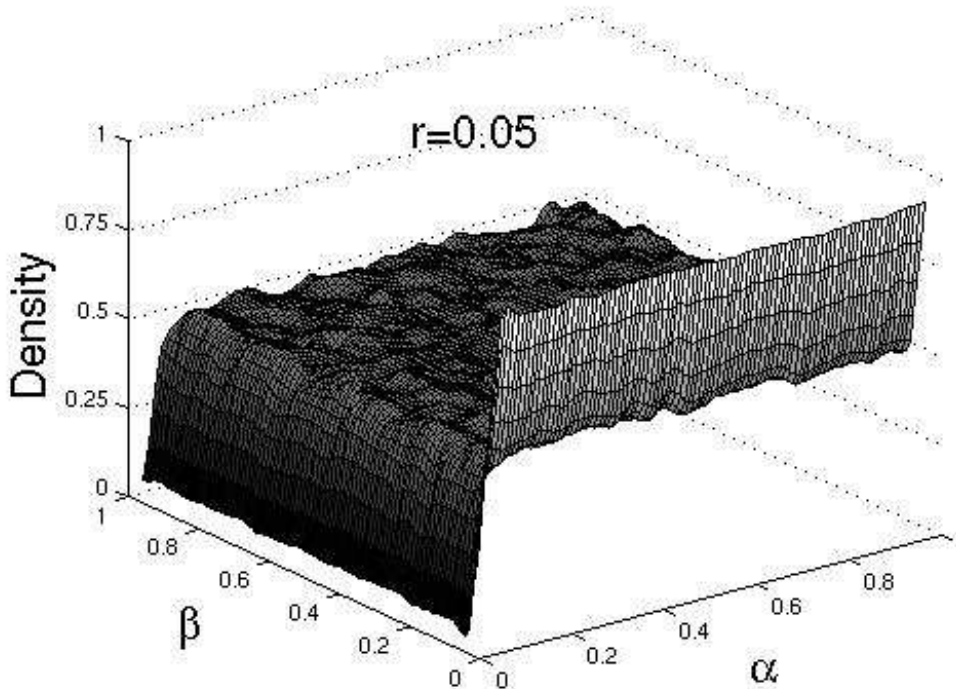


Fig. 9. Current versus the boundary and injection rates α and β , obtained through Monte Carlo simulations for parameter values $N = Lw = 128 * 10$ sites, $r = 0.05$, $P_{10} = 0.04$ and $P_{01} = 0.05$.

effects described in Refs. [34,35,36], where Langmuir kinetics competes with one-dimensional transport to yield a phase diagram with complex structure. We do not, however, address this interesting problem here.

4 Motor Microtubule Pattern Formation

The mitotic spindle of a dividing eukaryotic cell is a self-organized structure at the sub-cellular scale. Such structures are usefully thought of as patterns, by which we mean spatially inhomogeneous yet stable steady states, defined through the interaction of motors and microtubules. Experiments on centrosome-free fragments of the cytosol containing both motors and microtubules obtain self-organized radial structures called asters. Single asters, in addition to other complex patterns such as vortices, disordered aster-vortex mixtures and lattices of asters and vortices, are also seen *in vitro*, in experiments on mixtures of molecular motors and microtubules in a quasi-two-dimensional geometry[21].

What physical processes stabilize such structures? Direct molecular dynamics

simulations which incorporate any level of molecular-scale realism are currently incapable of tackling the pattern formation problem. One must then rely on approximate models for such systems, again keeping in mind the necessity of maintaining contact with biological reality: our models must be as simple as possible but no simpler. This problem has been studied extensively over the past 5 years or so with significant contributions from several groups [44,48,45,46,47]. This section summarizes work in this direction first presented in Ref. [7].

In this section, hydrodynamic equations of motion for a coarse-grained field representing the local orientation of microtubules as well as for local motor density fields are described. Our model treats motors attached to microtubules differently from motors which diffuse freely in solution. Motors which move on microtubules are referred to as “bound” motors, while those which diffuse in the ambient solvent are referred to as “free” motors. These are described by coarse-grained fields denoted by m_b and m_f respectively and obey different equations of motion.

We will take microtubules to be oriented by complexes of bound motors, yielding patterns at large scales. Our results are: We obtain a single vortex as a stable final state for large motor densities in some regimes. However, in other regimes, asters are favoured. A “lattice of asters” state is stabilized in our model through a low-order relevant term in the equation of motion for the microtubule orientation. On small systems, constraints due to confinement favour a small number of asters, whose number can be increased systematically as parameters are varied. We have also calculated the distribution of free and bound motors in asters and vortices obtained in our model; we derive an exponential decay of bound motor densities away from aster cores, modulated by a power-law in which the exponent of the power law depends in a non-universal way on dynamical parameters.

In the absence of interconversion terms changing a bound motor to a free motor, m_b obeys a continuity equation involving the current of motors transported along the microtubules. The free motor field m_f obeys a diffusion equation with a diffusion constant D . These two fields are coupled through mechanisms which convert “free” motors to “bound” motors and vice versa. We will take $\gamma'_{f \rightarrow b}$ and $\gamma'_{b \rightarrow f}$ to be the rates at which free motors become bound motors (“on” rate) and vice-versa (“off” rate).

Our aim is to write down a minimal set of equations capable of both describing the variety of patterns formed in such interacting motor-microtubule mixtures. We are guided both by symmetry, as is appropriate for a fully non-equilibrium system in which detailed balance based on rates derivable from a hamiltonian does not exist, as well as by considerations of simplicity: of an infinity of possible non-equilibrium terms allowed in our equations of motion,

we choose the simplest. In appropriately scaled units, the equations then are

$$\partial_t m_f = \nabla^2 m_f - \gamma_{f \rightarrow b} m_f + \gamma_{b \rightarrow f} m_b \quad (8)$$

$$\partial_t m_b = -\nabla \cdot (m_b \mathbf{T}) + \gamma_{f \rightarrow b} m_f - \gamma_{b \rightarrow f} m_b \quad (9)$$

$$\partial_t \mathbf{T} = C \mathbf{T} (1 - T^2) + m_b \nabla^2 \mathbf{T} + \epsilon \nabla m_b \cdot \nabla \mathbf{T} + \kappa \nabla^2 \mathbf{T} + S \nabla m_b \quad (10)$$

Free and bound motor density profiles in vortex and aster configurations can be obtained from the above equations. We set the time derivatives to zero *i.e.* $\partial_t m_f = \partial_t m_b = 0$, obtaining

$$\nabla^2 m_f - \nabla \cdot (m_b \mathbf{T}) = 0, \quad (11)$$

$$\nabla^2 m_f + (\gamma_{b \rightarrow f} m_b - \gamma_{f \rightarrow b} m_f) = 0. \quad (12)$$

For a single vortex *i.e.* $\mathbf{T} = \hat{\theta}$, we may assume radial symmetry and thus $m_f = m_f(r)$ and $m_b = m_b(r)$. We then obtain,

$$m_f(r) = c_1 + c_2 \ln(r), \quad (13)$$

where c_1 and c_2 are constants to be determined by boundary conditions and normalization. The relation $\gamma_{b \rightarrow f} m_b - \gamma_{f \rightarrow b} m_f = 0$ yields

$$m_b(r) = \frac{\gamma_{f \rightarrow b}}{\gamma_{b \rightarrow f}} (c_1 + c_2 \ln(r)). \quad (14)$$

For the motor distribution about a single aster *i.e.* $\mathbf{T} = -\hat{\mathbf{r}}$, we again assume radial symmetry for the bound and free motor densities. The boundary condition that the total motor current vanishes at the boundary implies

$$\partial_r m_f(r) = -m_b(r). \quad (15)$$

Thus we have

$$\partial_r^2 m_f + \left(\frac{1}{r} - \gamma_{b \rightarrow f}\right) \partial_r m_f - \gamma_{f \rightarrow b} m_f = 0. \quad (16)$$

The general solution to the equation above is a combination of confluent hypergeometric functions and can be written in terms of the two solutions of the hypergeometric Kummer equation, modulated by an exponential. It is useful to define a quantity p given by

$$p = \frac{1}{2} \left(1 - \frac{\gamma_{b \rightarrow f}}{\sqrt{\gamma_{b \rightarrow f}^2 + 4\gamma_{f \rightarrow b}}} \right). \quad (17)$$

Note that $0 \leq p \leq 0.5$ with $\gamma_{b \rightarrow f}, \gamma_{f \rightarrow b} \geq 0$.

The asymptotics is obtained using an integral representation for the appropriate hypergeometric functions. Our final result for the motor distribution about a fixed aster configuration is

$$m_f(r) \sim c_1 \frac{e^{-r/\xi}}{(\gamma_{b \rightarrow f}^2 + 4\gamma_{f \rightarrow b})^{p/2} r^p}$$

$$m_b(r) \sim c_1 \frac{e^{-r/\xi}}{(\gamma_{b \rightarrow f}^2 + 4\gamma_{f \rightarrow b})^{p/2} r^p} \left(\frac{p}{r} + \frac{1}{\xi} \right),$$

with $\xi^{-1} = \left| \frac{(\gamma_{b \rightarrow f} - \sqrt{(\gamma_{b \rightarrow f}^2 + 4\gamma_{f \rightarrow b})})}{2} \right| = \left| \frac{p\gamma_{b \rightarrow f}}{2p-1} \right|$. The correlation length ξ and the power-law exponent p depend on $\gamma_{f \rightarrow b}$ and $\gamma_{b \rightarrow f}$. We see that the bound motor density in the aster case has an exponential fall modulated by a power-law tail.

We also solve Equations 8,9 and 10 numerically on an $L \times L$ square grid indexed by (i, j) with $i = 1, \dots, L$ and $j = 1, \dots, L$. The equations for the free and bound motor densities are evolved using an Euler scheme. We impose the boundary condition that no current (either of free or bound motors) flows into or out of the system. This condition is easily imposed by setting the appropriate current to zero. The \mathbf{T} equation is differenced through the Alternate Direction Implicit (ADI) operator splitting method in the Crank-Nicholson scheme.

Our simulations are on lattices of several sizes, ranging from $L = 30$ to $L = 200$. We vary the motor density in the range 0.01 to 5 in appropriate dimensionless units. We work with two different types of boundary conditions on the T field. In the first, which we refer to as reflecting boundary conditions, the microtubule configuration at the boundary sites is fixed to point along the inward normal. In the second, which we refer to as parallel boundary conditions, microtubule orientations at the boundary are taken to be tangential to the boundary. In both these sets of boundary conditions, the state of the boundary T vectors is fixed and does not evolve. The total number of motors, initially divided equally between free and bound states and distributed randomly among the sites, is explicitly conserved.

Figures 10(a) – (d) depict four stable configurations obtained in different regimes of parameter space for an $L = 100$ lattice. Fig. 10(a) shows a disordered arrangement of microtubules obtained at very low motor densities ($m = 0.005$) with $\epsilon = 0.5$ and $S = 0$. Figure 10(b) shows an aster-vortex mixture obtained at $m = 0.01$ at the same values of ϵ and S . This figure is to be contrasted to Fig. 10(c), obtained at $m = 0.05$, taking $\epsilon = 5$ and $S = 0.001$. Note the absence of asters in this regime of parameter space. Finally, Fig 10(d), obtained with $m = 0.5$, $\epsilon = 1$ and $S = 1$, illustrates a lattice

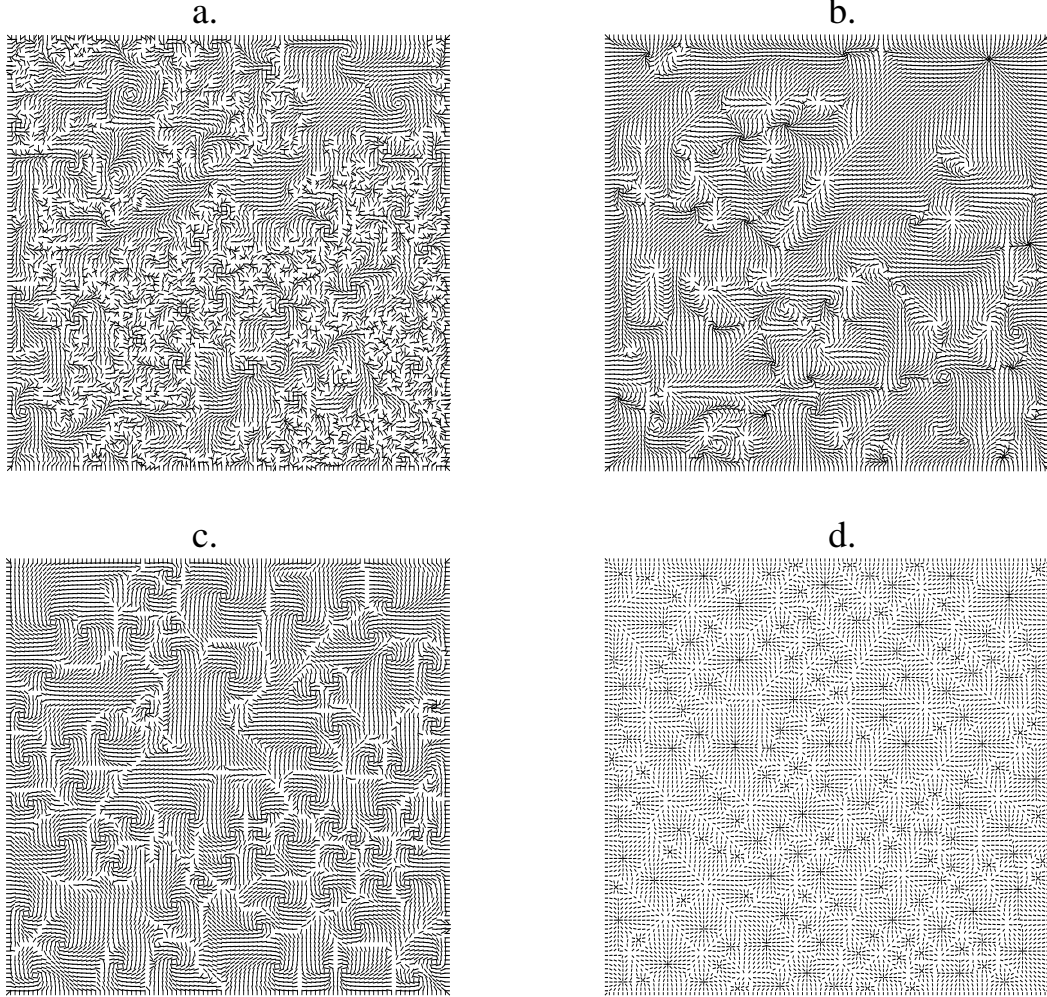


Fig. 10. Steady state configurations in our model at different parameter values (see text): (a) Disordered states obtained at very low motor densities [$m = 0.005$, $\epsilon = 0.5$ and $S = 0$]; (b) Aster-vortex mixture obtained at [$m = 0.01$, $\epsilon = 0.5$ and $S = 0$]; (c) Lattice of vortices at [$m = 0.05$, $\epsilon = 5$ and $S = 0.001$]; (d) Lattice of asters obtained at [$m = 0.5$, $\epsilon = 1$ and $S = 1$]

of asters, with asters being the only stable defects present. We can vary the sizes and numbers of asters obtained in configurations such as the one shown in Fig. 10(d), by changing S . A larger S yields a large number of small asters, while smaller values of S yield a smaller number of large asters[24].

Our results are summarized in Fig. 11 which shows the states which dominate in the three-dimensional space spanned by ϵ , S and m . For $S = 0$, we obtain disordered/aster-vortex mixture states at low motor density, which become a lattice of vortices at somewhat higher motor densities. Large values of ϵ ($\epsilon \geq 1$) yield well-formed vortex-like configurations while small ϵ yields structures better described as aster-vortex mixtures. At intermediate values of ϵ and m , spirals rather than vortices appear to dominate. At large m , with $S = 0$ and large ϵ , a single vortex is obtained[44,48].

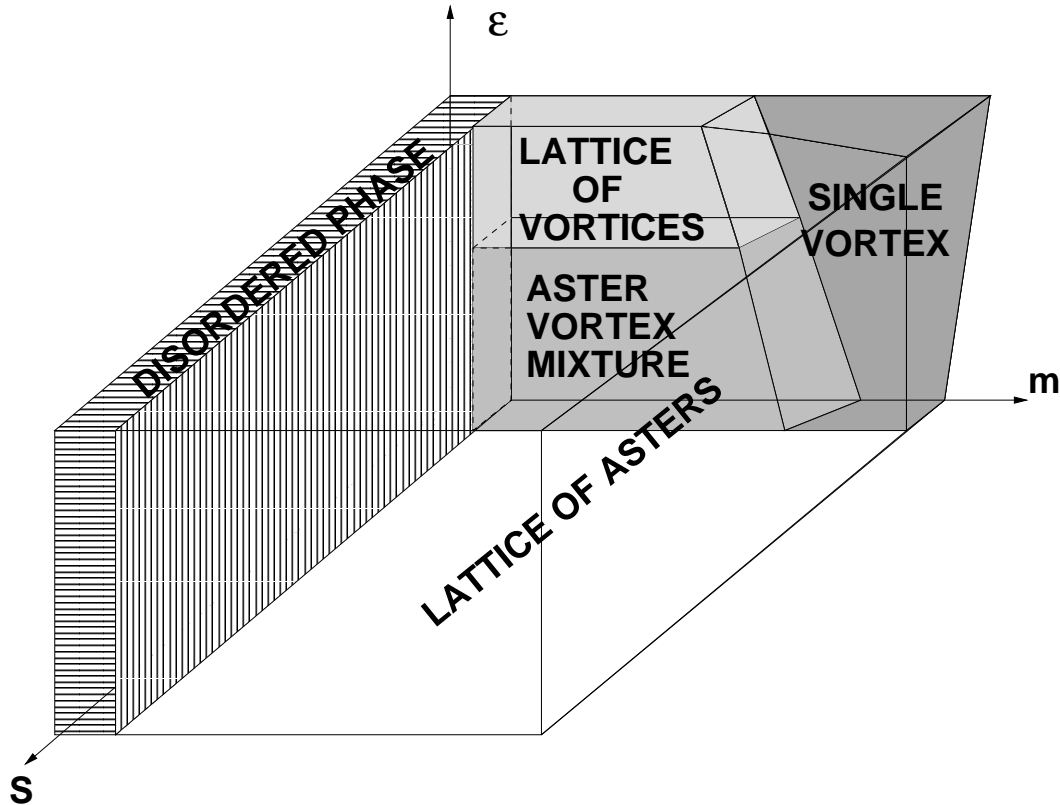


Fig. 11. Qualitative map of steady states illustrating how different states, the disordered state, the aster-vortex mixture state, the lattice of vortices state, the single vortex, the lattice of asters, dominate in different regimes of parameter space; for a definition of parameters see text. The parameter ϵ is plotted on the y axis, with the total motor density m plotted on the x axis. The parameter S extends out of the $\epsilon - m$ plane. Of the states shown, the lattice of asters is obtained generically for non-zero S (out of the plane of the figure), whereas the other states are associated with the $S = 0$ plane, although they appear to survive provided S is small enough.

For non-zero but small S , these states appear to continue out of the $S = 0$ plane but are rapidly replaced by a lattice of asters for larger S . A cut of Fig. 11 at finite S yields disordered states at small m and a lattice of asters at larger m . We can thus understand the sequence of patterns formed upon increasing m in mixtures of kinesin constructs with microtubules in terms of a trajectory which begins in the $S = 0$ (or S sufficiently small) plane in the disordered phase and transits between the aster-vortex mixture and the lattice of vortices (both of which lie in this plane) as m is increased. As m increases further and the effects of the S term become important, such a trajectory moves out towards non-zero S , encountering the lattice of asters.

We have also examined the effects of changing the motor processivity, a quantity proportional to the ratio of $\gamma_{f \rightarrow b}$ to $\gamma_{b \rightarrow f}$. Smaller values of this ratio are appropriate to molecular motors such as NCD. At $\gamma_{f \rightarrow b} = 0.005$, $\gamma_{b \rightarrow f} = 0.05$, we find that the disordered regime shown in Fig. 1 expands, so that at equiv-

alent values of m disordered states occupy much of the domain associated previously with the lattice of vortices. Whereas kinesins follow the sequence *disordered – lattice of vortices – aster vortex mixture – lattice of asters* as the m is increased, a mixture of microtubules with NCD motors bypasses the lattice of vortices altogether, transiting directly from the disordered state to the lattice of asters in the experiments[22]. In terms of Fig. 11, the expanded regime of disordered states for the NCD motor suggests that patterns such as the lattice of vortices and the aster-vortex mixture may be inaccessible at the motor densities at which the experiments are done, since the effects of the S term might be expected to dominate at large m .

It is interesting to note that the generic state which is obtained at large m is a lattice of asters for non-zero S , in contrast to the predictions of the earlier model of Lee and Kardar, which indicates that the large motor density state is always a single vortex. This feature, a direct consequence of the presence of the crucial $S\nabla m$ term, agrees with experiment. Further results, including a discussion of motor-motor interactions in the context of motor- microtubule pattern formation, qualitative “free-energy” based arguments for the stability of patterns and a detailed discussion of the effects of confinement can be found in Ref. [7].

5 Conclusions

The interacting thermal ratchet model discussed in the first part of this paper introduces a primitive level of biological realism into models for the motion of interacting motor proteins. While the model itself may not appear appreciably more realistic than the ASEP itself, the use of ratchet models generalized to include interactions is attractive, since such models incorporate the *true* reason for the symmetry breaking which occurs when molecular motors move unidirectionally in a Brownian environment. This reasoning is obscured in the currently popular ASEP-based models, where the symmetry breaking which leads to a non-trivial current is imposed by hand, through the definition of the hopping rates. Making the connection to ratchet models also facilitates the understanding of many issues relating to the coherence or reliability of transport[49] in motor systems as well as of efficiency in energy transduction[50]. The exclusion processes simply lack the necessary structure for such discussions to be meaningful.

We have also described calculations which relate to a non-equilibrium pattern formation problem: the formation of patterns in mixtures of microtubules and molecular motor constructs. The model is able to reproduce virtually all the patterns obtained in the experiments, but has the advantage over direct simulations that the number of parameters which need to be included is small. We

have also been able to derive many of the features of the patterns which form, including the sequence of patterns which are obtained as the motor density is increased. Our model rationalizes several features of the experiments, in many cases for the first time. These include: (i) the sequence of patterns obtained as the motor density is increased, (ii) the prevalence of the lattice of asters state and (iii) the difference in the sequence of patterns formed by conventional kinesins and the NCD motor. Many further features of these equations are currently being explored.

One final point relates to the nature of steady states which are obtained in the ratchet models generalized to include interactions between motors and has to do with the possibility of “robustness” in these models. Barkai and Leibler[42] and Alon *et. al.*[43] study the chemotaxis network of *E. Coli*, suggesting that this network exhibits *exact* and *robust* adaptation, over a wide range of variation of parameters. The robustness of adaptation in this case is an example of biochemical robustness, since it has its origins in specific features of the biochemical network underlying chemotaxis in *E. Coli*. The “tensegrity” of the cytoskeletal network of living cells can be thought of as another form of robustness. Such robustness of the structural elements in the cell to mechanical perturbations is distinct from biochemical robustness. It is thus interesting to ask the following question: Are other manifestations of robustness possible and are there biological situations in which they may be relevant?

We suggest another intriguing possibility for robust behaviour in biological systems, the *robustness of certain non-equilibrium steady states of biological systems to wide classes of physical perturbations*. A simple illustrative example in the context of the boundary driven interacting ratchet model is the independence of the steady state current on α and β for a very large range of such parameter values. This indicates that the current is insensitive to fairly large fluctuations in the input and output rates and is, moreover, pegged to the largest possible value it can take. The robustness here is for *physical* reasons, essentially having to do with the one-dimensional character of this steady state and the fact that the system can adjust its density profile to accommodate changes in the boundary driving rates. While allowing for Langmuir kinetics in the bulk in this specific case will generically destroy such behaviour in the thermodynamic limit, small systems should exhibit the same qualitative behaviour. It remains to be seen if such “steady-state robustness” or “physical robustness” is in fact a feature of some aspects of *in vivo* cellular function, independent of the models we contrive to describe such function. It would be interesting to look at other examples of non-equilibrium steady states in biological systems, possibly those which involve cell-scale flows (as, for example, in cell streaming), to see if this idea might find support.

6 Acknowledgements

The work described in the first section was done in collaboration with Yashar Aghababaie and Michael Plishke at Simon Fraser University, with research supported by the NSERC of Canada. The work described in the third part, relating to the motor-microtubule pattern formation problem was done in collaboration with Sumithra Sankararaman at the Institute of Mathematical Sciences and P.B. Sunil Kumar at the IIT, Madras and was partially supported by the DST (India). I am grateful to these collaborators for all I have learnt from them. At various stages, I have benefited from conversations with Michael Wortis, Jacques Prost, Mustansir Barma, Deepak Dhar, Arun Jayannavar, Madan Rao, Sriram Ramaswamy and Amit Kumar Bhattacharjee. I would also like to thank Debashish Chowdhury for organizing a very stimulating and topical conference on these and related issues where this work was presented.

References

- [1] S. Ramaswamy and M. Rao, *C.R. Acad. Sci Ser IV, Phys. Astrophys.* **2**, 818 (2001)
- [2] Y. Hatwalne, S. Ramaswamy, M. Rao and R. A. Simha, *Phys. Rev. Lett.*, **92** 118101 (2004)
- [3] J. Toner, Y. Tu and S. Ramaswamy, *Annals of Physics*, **318**, 170 (2005)
- [4] A.J. Koch and H. Meinhardt, *Reviews of Modern Physics*, **66**, 1481 (1994).
- [5] D. Chowdhury, A. Schadschneider and K. Nishinari, *Physics of Life Reviews*, **2**, 318 (2005).
- [6] Y. Aghababaie, G.I. Menon and M. Plischke, *Phys. Rev. E*, **59**, 2578 (1999).
- [7] S. Sankararaman, G. I. Menon and P. B. Sunil Kumar, *Phys. Rev. E*, **70**, 031905 (2004)
- [8] A.D. Mehta, M. Rief, J.A. Spudich, D.A. Smith and R.M. Simmons, *Science*, **283**, 1689 (1999)
- [9] J. Howard, *Mechanics of Motor Proteins and the Cytoskeleton*, Sinauer, (Sunderland, MA, U.S.A, 2001).
- [10] F. Jülicher, A. Ajdari and J. Prost, *Rev. Mod. Phys.* **69**, 1269 (1997).
- [11] P. Reimann, *Phys. Rep.*, **361**, 57, (2002).
- [12] F. Jülicher and J. Prost, *Phys. Rev. Lett.*, **75**, 2618 (1995)
- [13] F. Jülicher and J. Prost, *Phys. Rev. Lett.*, **78**, 4510 (1997)

- [14] S. Camalet, T. Duke, F. Jülicher and J., Prost, *Proc. Nat. Acad. Sci USA*, **97** 3183 (2000)
- [15] D. Dan, A. M. Jayannavar and G. I. Menon *Physica A*, **318**, 40 (2003)
- [16] I. Derényi and T. Vicsek, *Phys. Rev. Lett.* **75**, 374 (1995); I. Derényi and A. Ajdari, *Phys. Rev. E* **54**, R5 (1996).
- [17] K. Nishinari, Y. Okada, A. Schadschneider and D. Chowdhury, *Phys. Rev. Lett.*, **95** 118101 (2005)
- [18] J. Krug, *Phys. Rev. Lett.*, **67** 1882 (1991)
- [19] B. Derrida, E. Domany and D. Mukamel, *J. Stat. Phys.*, **69** 667 (1992); G. Schutz and E. Domany, *J. Stat. Phys.*, **72** 277 (1993); B. Derrida *et. al.* *J. Phys. A*, **26** 1493 (1993).
- [20] R.B. Stinchcombe, *Advances in Physics* **50** 431 (2001).
- [21] F. Nédélec, T. Surrey, A. C. Maggs and S. Leibler, *Nature* **389**, 305 (1997).
- [22] T. Surrey, F. Nédélec, S. Leibler and E. Karsenti, *Science* **292**, 1167 (2001).
- [23] F. Nédélec and T. Surrey, *C. R. Acad. Sci. Paris, Série IV*, 841 (2001).
- [24] F. Nédélec, T. Surrey, A. Maggs, *Phys. Rev. Lett* **86**, 3192 (2001).
- [25] F. Nédélec, *Journal of Cell Biology*, **158**, 1005 (2002).
- [26] F. Nédélec, T. Surrey and E. Karsenti, *Current Opinion in Cell Biology* **23**, 118 (2003).
- [27] R. Heald, R. Tournebize, A. Habermann, E. Karsenti, and T. Hyman, *Jour. Cell Biol.* **138**, 615 (1997); R. Heald, R. Tournebize, T. Blank, R. Sandaltzopoulos, A. Hyman, and E. Karsenti, *Nature* **382**, 420 (1996).
- [28] M. Kardar, G. Parisi and Y. C. Zhang, *Phys. Rev. Lett.* **56**, 889 (1986).
- [29] See A.-L. Barabási and H.E. Stanley, *Fractal Concepts in Surface Growth*, (Cambridge University Press, 1995) for a review of much of this work, especially in the context of nonequilibrium surface growth.
- [30] H. van Beijeren, R. Kutner and H. Spohn, *Phys. Rev. Lett.* **54**, 2026 (1985).
- [31] D. Dhar, *Phase Transitions*, **9**, 51 (1987).
- [32] L-H. Gwa and H. Spohn, *Phys. Rev. A*, **46**, 844 (1992).
- [33] M. Plischke, Z Rácz and D. Liu, *Phys. Rev. B* **35**, 3485 (1987).
- [34] A. Parmeggiani, T. Franosch and E. Frey, *Phys. Rev. Lett.*, **90**, 86601 (2003)
- [35] A. Parmeggiani, T. Franosch and E. Frey, *Phys. Rev. E*, **70**, 46101 (2004)
- [36] H. Hinsch, R. Kouyos and E. Frey, *cond-mat/0512447*

- [37] R. Lipowsky, S. Klumpp and T.M. Nieuwenhuizen, *Phys. Rev. Lett*, **87**, 108101, (2001)
- [38] T.M. Nieuwenhuizen, S. Klumpp and R. Lipowsky, *Europhys. Lett*, **58**, 468 (2002).
- [39] T.M. Nieuwenhuizen, S. Klumpp and R. Lipowsky, *Phys. Rev. E*, **69**, 061911 (2004).
- [40] S. Klumpp, A. Mielke and C. Wald, *Phys Rev E*, **63**, 031914 (2001).
- [41] S. Klumpp, T.M. Nieuwenhuizen and R. Lipowsky, *Physica E*, **29**, 380 (2005).
- [42] N. Barkai and S Leibler, *Nature* (London), **387**, 913 (1997)
- [43] U. Alon, M.G. Surette, N. Barkai and S. Leibler, *Nature*, (London), **397** 168 (1998)
- [44] H. Y. Lee and M. Kardar, *Phys. Rev. E* **64**, 056113 (2001).
- [45] T. B. Liverpool and M. C. Marchetti, *Phys. Rev. Lett*, **90**, 138102 (2003); F. Ziebert and W. Zimmermann, *ibid.* **93**, 159801 (2004).
- [46] K. Kruse *et al.*, *Phys. Rev. Lett* **92**, 078101 (2004)
- [47] I. S. Aranson and L. S. Tsimring, *Phys. Rev. E*, **71**, 050901(R) (2005)
- [48] J. Kim, Y. Park, B. Kahng, and H.Y. Lee, *Jour. Kor. Phys. Soc.* **42**, 162 (2003).
- [49] J.A. Freund and L. Schimansky-Geier, *Phys. Rev. E*, **60** 1304 (1999); T. Harms and R. Lipowsky, *Phys. Rev. Lett*, **79**, 2895 (1997); R. Krishnan, D. Dan and A.M. Jayannavar, *Physica A*, **354**, 171 (2005)
- [50] A. Parmeggiani, F. Jülicher, A. Ajdari and J. Prost, *Phys Rev. E*, **60**, 2127 (1999)